IOP Publishing Journal of Physics G: Nuclear and Particle Physics
J. Phys. G: Nucl. Part. Phys. **47** (2020) 035204 (14pp) https://doi.org/10.1088/1361-6471/ab50c9

Determination of local muon flux using astronomical Charge Coupled Device

Pantea Davoudifar[1] **and Zahra Bagheri**[1,2]

[1] Research Institute for Astronomy and Astrophysics of Maragha (RIAAM), University of Maragheh, Maragheh, Iran
[2] Institute for Research in Fundamental Sciences (IPM), School of Astronomy, Tehran, Iran

E-mail: Bagheri.zahra87@gmail.com

Received 18 May 2019, revised 17 October 2019
Accepted for publication 24 October 2019
Published 6 February 2020

Abstract

As an abundant component of secondary cosmic rays at the Earth, muons carry significant data, such as information on mass number of primary particles producing extensive air showers. Anyhow, the total muon flux is an important observable in many phenomena, for example it is suggested that the muon flux is influenced by the level of solar activity at the Earth, while the neutrino anomaly and hadronic interaction models are studied through the products of muon decay. As a result a part of any cosmic ray detector is designed to observe muons, count and evaluate their energy and angular distribution. Thus a simple method was started in Research Institute for Astronomy and Astrophysics of Maragha, University of Maragheh, to study the recorded tracks of particles by an astronomical CCD at 1478 m above sea level. To analyze recorded data and determine the muon flux from experiments, the flux of secondary atmospheric muons simulated with CORSIKA code (version 6.9) to study the muon angular distribution for our geographical location (latitude: 46.2534°E, longitude: 37.3892°N). The data used here were gathered during a ground run on 4 months (of 2016 and 2017), at Maragheh, Iran. The paper presents numerical results of the muon's flux obtained at 1478 m above sea level which is in good agreement with expected values from simulations. The results were compared with experimental data from different experiments.

Keywords: CCD, cosmic rays, muon, CORSIKA, detector, simulation

(Some figures may appear in colour only in the online journal)

1. Introduction

Interactions of high-energy charged particles with the Earth's atmosphere produce showers of secondary particles called extensive air shower (EAS) [1]. Near the top of the atmosphere EASs are mainly consist of neutral and charged pions. Pions are very unstable, for example $\pi^0 \rightarrow 2\gamma$ occurs in less than 10^{-16} s (via electromagnetic force) and $\pi^{\pm} \rightarrow \mu^{\pm} + \nu_{\mu}(\overline{\nu}_{\mu})$, in less than 30 ns (via weak force). Muons decay with a longer mean lifetime (2.2 μs) according to: $\mu^{\pm} \rightarrow e^{\pm} + \nu_e(\overline{\nu}_e) + \overline{\nu}_{\mu}(\nu_{\mu})$ (via weak force). Positive muons can only decay, while negative muons can be trapped in atomic orbit so that they may decay or be absorbed by atomic nuclei which reduce their mean lifetime [2].

Due to relativistic time dilation in the Earth's reference frame, many of the muons are able to reach at the ground as a main component of charged particle at sea level [3]. Especially total muon number in an EAS is nearly constant after the shower maximum. Generated muons are usually not proliferated, intensity peak is around altitude of 10 km for $E \geqslant 1$ GeV and an exponential decrease in intensity occurs below 500 g cm^{-2} ($\approx$6 km) [4].

In this study we aimed to use and calibrate our astronomical Charge Coupled Device (CCD) to count the local muon numbers, as for our space weather studies we need to verify the results of our method of calculating the secondary particles on the Earth.

It was seen that the flux of muons on the Earth is affected by large flares, and also is varied at different seasons. At low energies ($\sim$1 GeV) the observed seasonal effects in muon flux are mostly due to muon decay [5, 6]. Today, the development of high energy interaction models and studying the phenomena such as neutrino anomaly are studied via muon decay [7, 8].

In comparison of multi-segmented scintillator hodoscopes, sets of ion chamber and photographic plates and other large detectors, CCDs are highly sensitive. This feature is an advantage when detecting high energy particles [9] in different heights and underground [10]. As muons are low interaction particles, their paths through CCDs are recorded as straight lines, which make it possible to detect them easily from recoiling electrons and alpha particles. In most of the underground detectors CCDs are the key instruments for detecting muons [11]. Other advantages of using CCDs are their low cost, being compact, low weight and have a variety of sizes from very small to large which make it possible to use CCDs in many places as scientific detectors. For example it was possible for Transition Region and Coronal Explorer (TRACE) [12] to record high energy particles in large eruptions from the Sun during its mission. Because of their capability of recording charged particle traces, now CCDs are widely used as particle detectors [13, 14].

In order to determine a local muon flux, we recorded the particle tracks using a CCD at Research Institute for Astronomy and Astrophysics of Maragha, University of Maragheh. To complete this method, using CORSIKA software [15], a simulation was carried out to study the angular distribution of muons at the detector level.

2. Experimental arrangement in RIAAM

We have used a QHYCCD QHY6. The CCD is arranged horizontally on a wooden desk, under metal roof of 0.6 cm of aluminum (2 parallel plates of aluminum 1050, 2.71 g cm^{-3}, 3 mm, spaced nearly 4 cm), connected to a computer. CCD was sealed with black tape and were held in a polyethylene box with an approximate diameter of $\sim$3 mm to be isolated from visible light and to reduce both photon and low energy electron events. The location of experiment was on the third floor of the Research Institute for Astronomy and Astrophysics of

Maragha, University of Maragheh. (Maragheh city latitude, longitude and elevation are: 46.267°E, 37.400°N and elevation of 1467.0 m relative to mean sea level reported by 'Integrated Surface Database Station History' [16]—an elevation value of 1477.7 m was a mean value reported by the Iran Meteorological Organization [17], we have used 1478 m for simulation corresponding to an average atmospheric depth of ∼867 g cm^{-2} based on US standard atmosphere [18].)

The images were recorded in local daytime (i.e. 6 am–6 pm), each image was recorded in a period of 10 min 72 image each day. The temperature was constant on 25 °C. Images were recorded for two periods of 1 November 2016 to the end of December 2016, and 1 May to the end of June 2017.

This type of CCD uses an image sensor Sony™ ICX 259 AL monochrome, interline, interlaced, EXView HAD CCD™, interlaced, EXView HAD CCD™ [19, 20], $1/3''$ (diagonal 6 mm), with the effective pixel number of 752(H)*582(V) ∼0.4 Mpixel and unit cell size 6.50 μm (H), 6.25 μm (V).

The dimension of CCD chips (including 16 pin DIP (Plastic)) are: chip size 6.00 mm (H) × 4.96 mm (V). For our calculations the dimension of active area was considered using the 'effective pixels'. The CCD uses a silicon substrate material [19], for which we considered an 'effective region thickness' (or 'active region thickness') of ∼20 μm [13, 21] (it is approximately equivalent to the length of 3 pixels in our CCD, figure 4).

Image data is stored in tables of 800*596 (column and rows with 5 extra columns on left), with position of optical black are H: Front 3, rear 40; V: Front 12, rear 2 [19]. The extra columns on the left and the columns of optical black pixels were removed to have effective number of pixels 752(H)*582(V). (i.e. $800 - 5 - 3 - 40 = 752$, $596 - 12 - 2 = 582$).

Both positive and negative muons were counted in the recorded long dark images.

Lots of the images were inadequate and of course not all of them included an event. For November 2016, 59 images were chosen as usable (high quality images with no significant solar occurrence simultaneously). There were 230 events on those images (straight lines, worm and spots). Figure 1 shows frames taken by our CCD after 10 min of exposure.

3. Data analysis and method

For each pixel there is a number that corresponds with the stored luminosity on that pixel. Image data, using FV Interactive FITS File Editor [22] is stored in text tables, 596 rows and 800 columns. Using IDL coding [23] appropriate filter remove dark current, bias, flat fielding and the table dimension properly reduced to 752(H)*582(V) by removing the extra columns on the left and the columns of optical black pixels. The pixel values is normalized to grayscale via equation (3.1).

$$\mathrm{DATAPROC}(I, J) = \frac{255 \times \log(1 + \mathrm{DATAPROC}(I, J))}{\log(1 + R)}. \tag{3.1}$$

DATAPROC is the array contains the brightness of pixels in grayscale. I and J are indexes which provide access to different pixels of images (i.e. row and columns). R is the corresponding value of the brightest pixel.

Simply, we start to recognize maximum of 10 tracks (by default) from the new array of (3.1) (the number of 10, was the maximum number of tracks that we found experimentally. i.e. we saw no more than 10 tracks in one image).

Step 1:

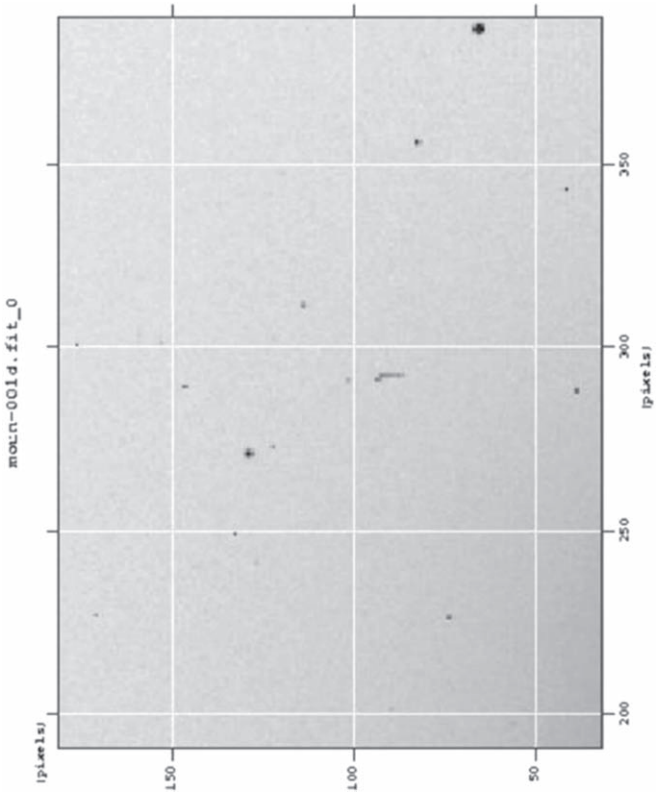

Figure 1. Raw image recorded by CCD, magnification 8 of FV software.

To find the tracks, first the brightest pixel of the image is found, then a 21*21 slice of the image is removed in which this bright pixel is located exactly in the middle (i.e. at 11th column and 11th row of this slice. Here the dimension of slice is decided considering a best value to include the maximum observed track length).

In the main image, the pixels in the position of this slice are replaced by zeros.

Then the second slice is removed as above and this procedure continues to remove and save up to 10 events.

Step 2:

For each of these 10 slices, first we detect the type of tracks (straight-line or not).

As the brightness distribution of pixels is nearly Gaussian, to observe the tracks more simply we considered a filter defining a threshold of $(1 - 1/2e) \times R'$ in which R' is 'the value of brightest pixel in the slice', 'e' is Euler's number. Then the pixel values for which the intensities are less than $(1 - 1/2e) \times R'$, were replaced by zeros and other pixel values were set to 1. (In fact we tried other threshold values, for example $(1 - 1/e) \times R'$ and $(1 - 1/3e) \times R'$ etc, but the above threshold gave the best result.) The new slice (21*21) named 'SUBN(K,L)' in which K and L correspond to the image number and the number of detected track (i.e. 1:10),] respectively.

Whenever with these conditions, 3 or more neighboring pixels are found, we verify if the track is a straight line or not:

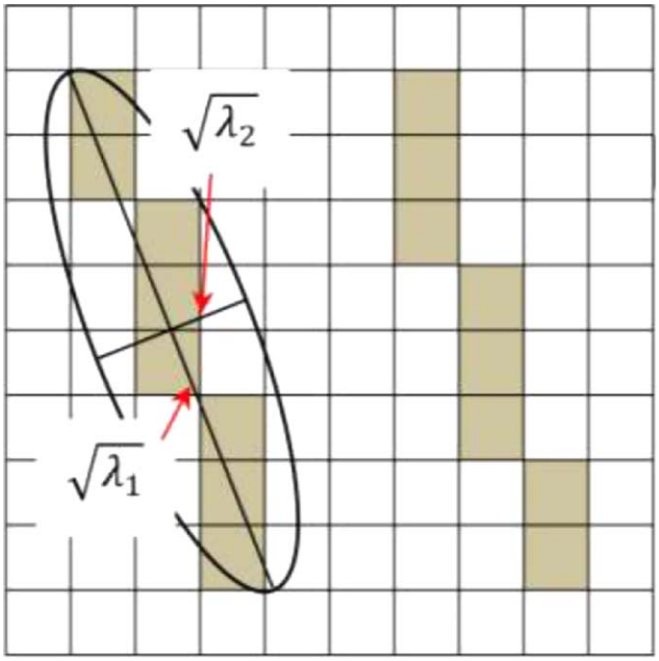

Figure 2. Drawn ellipse on a track to define λ_1 and λ_2.

Find the start and the end of the track and connect them with a line. By using ceiling and floor mathematical functions, any possible connecting line would be created. Then the pattern(s) of line will be compared with the points of the track one by one.

At stage 1 the tracks are divided to two categories (lines and others). Lines are equivalent to muon tracks. For all the tracks the values of relevant parameters of an ellipse will be calculated.

The method for this part is using a 'density matrix'. The only specification which is used here is the location of bright pixels of the track.

The density matrix is a 21*21 matrix for which the track pixels have a value of 1 and all other elements are set to zero.

We draw an ellipse with bright pixels inside/or on its perimeter.

Mathematically to find this ellipse, first one should find the center of mass of the track as:

$$\begin{cases} X_{CM} = \dfrac{\sum_{j=0}^{20}\sum_{i=0}^{20} X_i M_{i,j}}{M_{\mathrm{TOTAL}}} \\ Y_{CM} = \dfrac{\sum_{i=0}^{20}\sum_{j=0}^{20} Y_j M_{i,j}}{M_{\mathrm{TOTAL}}} \end{cases} \tag{3.2}$$

(for which the values of weight functions, $M_{i,j}$, are 0 and 1) and make the 'density matrix' diagonal. Now the center of mass is the center of ellipse and semi major and semi minor axes are calculated from eigenvalues as:

$$\begin{cases} \text{length of semi major axis} = 2\sqrt{e_1} \\ \text{length of semi minor axis} = 2\sqrt{e_2} \end{cases}. \tag{3.3}$$

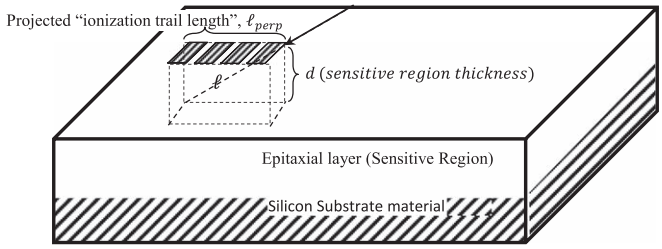

Figure 3. The schematic of a muon track in a CCD.

Thus λ_1 and λ_2 are (figure 2):

$$\begin{cases} \sqrt{\lambda_1} = 2\sqrt{e_1} \\ \sqrt{\lambda_2} = 2\sqrt{e_2} \end{cases} \Rightarrow \begin{cases} \lambda_1 = 4e_1 \equiv (\text{length of semi major axis})^2 \\ \lambda_2 = 4e_2 \equiv (\text{length of semi minor axis})^2 \end{cases}, \tag{3.4}$$

where e_1 and e_2 are 2 eigenvalues ($e_1 > e_2$).

The quantity of 'Ellipticity' is defined by ellipticity $= 1 - \lambda_2/\lambda_1$. We anticipate that the tracks belonging to the exactly straight lines have semi minor axis equivalent to zero, and as the track is far from the straight line, the semi minor axes value is larger (with definition) and also ellipticity is closer to zero.

3 For simplicity all the patterns equivalent with a spot are pre-defined and 'others' which are not line or spot are considered as worm tracks.

Step 3:

By definition the 'number of counts' in a charge coupled device is the number of electron–hole pairs which is conventionally scaled by the active region thickness divided to the track length [24]. Generally the number of pairs is $n_{\text{pairs}} = E_{\text{deposited}}/\Delta E$. For silicon $\Delta E \sim 3.6$ eV [25] (3.68 eV [24]). Deposited energy for charged particles is integrated energy lose over the track length [26]. In a thin ($\sim$20 μm) layer of silicon the average value of energy lose was experimentally estimated as $\mathrm{d}E/\mathrm{d}x = \left(\frac{80}{\beta^2}\right)e$–$h$ pairs $\mu\mathrm{m}^{-1}$ [27] which is ~ 80 e–h pairs $\mu\mathrm{m}^{-1}$ for a minimum ionizing particle (i.e. $\beta \sim 1$).

It is convenient to use the projected 'ionization trail length (ℓ)' (i.e. ℓ_{perp}) in figure 3 and scale the number of counts to per thickness of epitaxial layer (i.e. sensitive region thickness, d). The value called 'perpendicular counts' [28] and considering the above definition is formulated as:

$$\text{Perpendicular counts} = \text{counts} \times d/\ell, \tag{3.5}$$

where d/ℓ, shows the angle of incidence [13].

4. Simulation for angular distribution of muons on observation level

For our experimental arrangement it is impossible to distinguish the muons that radiate vertically to CCD from the photons (without any tools like a calorimeter). Also in the definition of a track we considered at least 3 neighboring pixels to examine the possibility of the existence of a line (step 2 of section 3). We do not count the spots to make certain. But using simulation, we can stipulate the correct coefficient for this CCD.

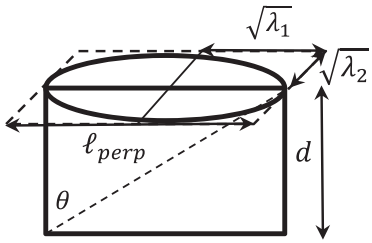

Figure 4. Simple geometry for calculating the minimum zenith angle of muons according to our applied algorithm. '*d*' is the sensitive region thickness of CCD in terms of pixels ($\sim 20\ \mu$m).

According to the applied algorithm, if we have 3 back-to-back squares which are bright (after the elimination of the background noise and applying filters) and if this track being considered as a straight line, it would count as muon track. Thus we miss any muons which produce a track with a lower dimension (i.e. 2 pixels). As a result we can consider the least zenith angle below which we do not detect possible muons.

According to figure 4, we have counted muons entering the CCD with zenith angles greater than about 33°. Therefore, we need to simulate the secondary muon flux to obtain the percentage of lost muons in our counting procedure.

We simulated the propagation of high energy protons in the atmosphere using CORSIKA program (version 6.9) [15, 18] with QGSJET [29], GHEISHA [30] and a flat atmosphere. To do this, the total number of 10 000 showers were simulated in energy range of 10^9–10^{16} eV (1000 showers for each energy range from 10^8 to 10^{18} eV but the lowest range produced no secondaries for our observation level. Also at the highest range the weighting parameter eliminated the contribution of higher energies in producing a local muon flux). Primary particles (proton) have considered with an incidence zenith angle of $0^\circ \leqslant \theta \leqslant 70^\circ$ and azimuth of $-180^\circ \leqslant \varphi \leqslant 180^\circ$. The value of the Earth's magnetic field of $B_X = 26.875$ nT, $B_Z = 40.07$ nT and the observation level 1478 m were considered.

The weighting factors were calculated from Alcaraz *et al* [31] (downward fluxes, tables 2 and 3 therein) up to few 100 GeV and for the higher energies we have used the universal cosmic ray flux of $\propto E^{-2.7}$ (i.e. considered those higher energies as galactic) [32]. To calculate the weighting factors we have used $\varepsilon(E_j) = I(E_j)\Delta E_j / \sum_{j=i}^{f} I(E_j)\Delta E_j$, in which $I(E_j)$ is the value of differential flux in *j*th energy bin in $(\mathrm{m^2\ sr\ s\ MeV})^{-1}$, ΔE_j is the width of *j*th energy bin in (MeV) and $\sum_{j=i}^{f} I(E_j)\Delta E_j$ is the total number of primary particles in whole energy range ($E_i = 1$ GeV, $E_f = 10^7$ GeV) in $(\mathrm{m^2\ sr\ s})^{-1}$. Thus for each energy bin we have a different weighting factor. As a result for data from [31] we have $\varepsilon(E_1) \sim 0.0017$ for the first energy bin (0.85–1.15 GeV) and $\varepsilon(E_{31}) \sim 0.0008$ for the 24th energy bin (162.29–199.06 GeV) of AMS01 data.

In our simulation, we assumed that the collisions occur randomly on a hypothetical surface above the atmosphere with an area of $\frac{1}{144}$ steradians as Bobik *et al*, was suggested [33] (i.e. particles hitting the atmosphere out of this surface do not contribute in the flux of secondary particles for the desired geographical location). The positions of particles were selected randomly on this surface.

After applying the proper weighting factors on CORSIKA outputs, we counted the number and angular distribution of generated muons on our observation level.

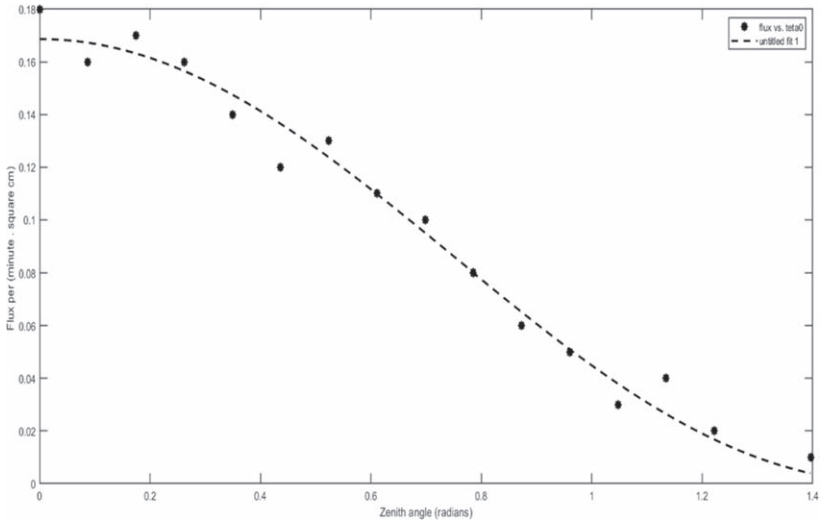

Figure 5. Angular distribution of cosmic muons at Maragheh measured by simulation.

Table 1. Simulation result of muon angular distribution in Maragheh.

Zenith angle intervals (°)	Flux ($cm^{-2}\,min^{-1}$)	Zenith angle intervals (°)	Flux ($cm^{-2}\,min^{-1}$)
0–5	0.18 ± 0.02	40–45	0.10 ± 0.02
5–10	0.16 ± 0.01	45–50	0.08 ± 0.01
10–15	0.17 ± 0.01	50–55	0.06 ± 0.01
15–20	0.16 ± 0.02	55–60	0.05 ± 0.01
20–25	0.14 ± 0.02	60–65	0.03 ± 0.01
25–30	0.12 ± 0.02	65–70	0.04 ± 0.02
30–35	0.13 ± 0.01	70–80	0.02 ± 0.01
35–40	0.11 ± 0.02	80–90	0.01 ± 0.01

Bin widths of 5° were considered for zenith angle (for example all muons with zenith angles 0°–5° were counted for which the azimuth was a free parameter).

$$\theta = \tan^{-1}\frac{\sqrt{{p_x}^2 + {p_y}^2}}{p_z}, \quad \varphi = \tan^{-1}\frac{p_y}{p_x}. \tag{4.1}$$

The results of our simulation (in 5° zenith intervals) in Maragheh were shown in table 1 and figure 5.

For $\theta \leqslant 75°$, the zenith angle (θ) dependence of the cosmic muon intensity is given by the expression [34, 35]:

$$I_\mu(\theta) = I(0°)\cos^n\theta, \tag{4.2}$$

where $I(0°)$ is the muon intensity in ($cm^{-2}\,min^{-1}$) at 0° and n is a function of the muon momentum. The exponent $n = 1.95 \pm 0.08$ for muons with energies above 1 GeV is in good agreement with Grieder [36]. The function which is given to the inputs for fitting is:

Table 2. Results for 3 sample events.

Event's kind	$\sqrt{\lambda_2}$ (pixels)	ℓ_{perp} (pixels)	Perpendicular count
Muon	0.4	~ 6	33 925
Spot	1.0	$\sim$2.1	12 597
Worm-shaped	0.9	$\sim$1.6	8120

$$I_\mu(\theta) = I_0 \cos^n \theta \tag{4.3}$$

which gives coefficients (with 95% confidence bounds) based on the simulation results:

$$\begin{cases} I_0 = 0.176\ (0.1606,\ 0.1767) \\ n = 2.101\ (1.867,\ 2.434) \end{cases}. \tag{4.4}$$

According to the results of simulation $I(0°) \sim 0.18$ (cm^{-2} min^{-1}) and flux of all muons at observation level is:

$$I_\mu = \int_0^{\pi/2} I_0 \cos^2\theta \mathrm{d}\theta \sim 1.56 \pm 0.05\ (\text{cm}^{-2}\ \text{min}^{-1}). \tag{4.5}$$

Considering the reported value by Bobik *et al* [33]:

$$\begin{cases} \mu^+ \sim 14.1 - 22.2 \text{ particles per(m}^2 \text{ sr s)} \\ \mu^- \sim 10.9 - 18.4 \text{ particles per(m}^2 \text{ sr s)} \end{cases} \equiv \begin{cases} \mu^+ \sim 0.5 - 0.8 \text{ particles per(cm}^2 \text{ min)} \\ \mu^- \sim 0.4 - 1.7 \text{ particles per(cm}^2 \text{ min)} \end{cases}$$

the total values are:

$$\mu^\pm \sim 0.9 - 2.5 \text{ particles per(cm}^2 \text{ min)}$$

which indicates the accuracy of our simulation method.

Further investigation of the simulation result shows that about half of the muons are missed in counting method as:

$$\int_0^{33\circ} I_0 \cos^2\theta \mathrm{d}\theta / \int_{0\circ}^{90\circ} I_0 \cos^2\theta \mathrm{d}\theta \sim 1/2. \tag{4.6}$$

Therefore, as we have indicated in simulation of muon angular distribution at the level of Maragheh, detected muons with zenith angles between 30° and 90° by our balanced detector are half of the total muons. According to the applied angular accuracy in our simulation, the error is less than: $\Delta_{I_\mu} \sim 0.01$ (cm^{-2} min^{-1}).

5. Calculations and the results

In equation (3.5) and figure 3, $\ell = \sqrt{d^2 + \ell_{\text{perp}}{}^2}$, thus:

$$\text{Perp. counts} = \text{counts} \times \frac{1}{\sqrt{1 + (\ell_{\text{perp}}/d)^2}}.$$

For our CCD, ℓ_{perp} is the given track length (is calculated from the recorded tracks in μm) d is estimated $\sim$20 μm and counts were estimated to be ~ 80 e–h pairs μm^{-1} [27] (i.e. $\sim$16000 e–h pairs per 20 μm).

For three different kinds of events 'Muon', 'Spot' and 'Worm-shaped', we show the values of perpendicular count 3 sample events in table 2:

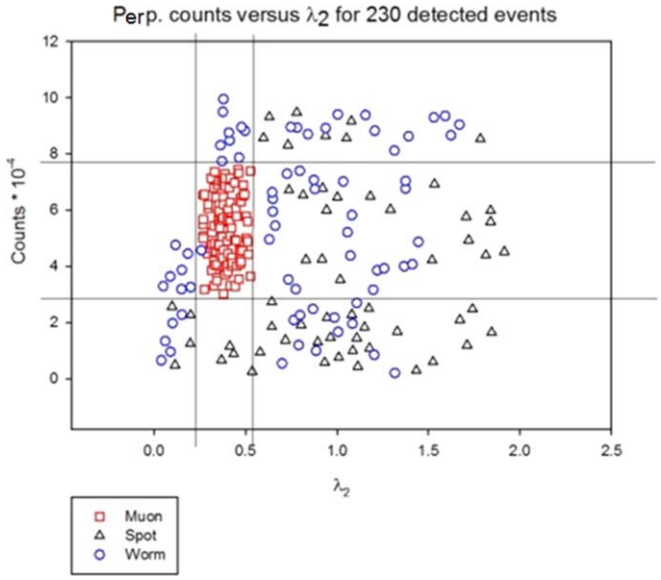

Figure 6. Distribution of 'perp counts' as a function of λ_2.

In our analysis the values of λ_2/λ_1 was smaller than 0.25 for muon's track which means an ellipcitity of $0.75 <$ ellipcitity < 1. Most of the recorded muons in this research (88 events from 102) had an ellipticity between 0.9 and 1. It must be noted that muons with entrance angles near to vertical ($\lambda_2/\lambda_1 \sim 1$) were not counted because we could not distinguish them from photons.

The perpendicular count as a function of λ_2 for our 230 events is shown in figure 6.

Though we have not recorded many events the distribution of 'perp counts' shows a muon box

$$\begin{cases} 0.25 < \lambda_2 < 0.53 \\ 2.8 \times 10^4 < \text{perp.count} < 7.9 \times 10^4 \end{cases}. \tag{5.3}$$

In figure 7, there are some samples of possible tracks along with their parameters normalized according to pixel unit.

Our results led us to calibrate our consumed CCD for detecting muons. Various diagrams can be used to calibrate the CCD. For example, diagram of the perpendicular counts in terms of $\sqrt{\lambda_2}$ or ellipticity diagram. In this work we used perp count diagram.

The active pixels of our CCD are 756*582 as presented in the paper.

The pixel dimension is also presented 6.5*6.25 $(\mu m)^2$.

Thus the dimension of active region is 752*6.5 (in μm) and 582*6.25 (in μm) and the total area is 4888 μm (0.4888 cm) * 3637.5 μm (0.36375 cm): ~0.18 $(cm)^2$.

The number of the muon tracks that we found for first month was 88, the total time of recording was 59*10 min (each image taken in recorded in 10 min).

So the value is 88/(590*0.18) ~0.83 particles per (min cm^2)

$$f = \frac{88}{590 \times 0.18} \sim 0.83 \frac{\text{particles}}{\text{min cm}^2}. \tag{5.4}$$

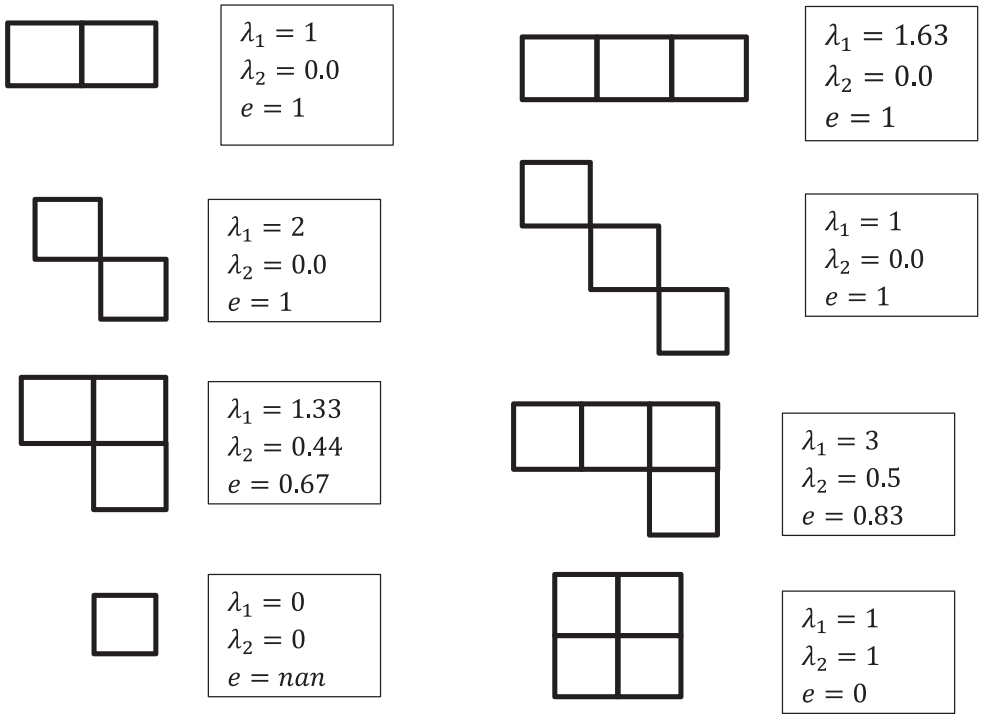

Figure 7. Sample of possible tracks along with their parameters.

According to the simulation results, this flux is half the total flux of the muons at the observation level, which means the local flux of the muons at the height of the Maragheh is equal to:

$$f \sim 1.6 \frac{\text{particles}}{\text{min cm}^2}. \tag{5.5}$$

6. Discussion

In his 1986, Mackay reported [37] the rates of 10 $\text{cm}^{-2}\,\text{min}^{-1}$ for ground level cosmic rays. Later Florentin–Nielsen and Anderson [38] reported a reduction of 33% in surface rate of the observed flux 37 m below ground level.

The total flux of muons is reported in other researches for different geographical location and altitudes. For example: Haino *et al* [39], reported the absolute flux of muons at sea level. Considering atmospheric muon flux in the range 0.6–400 GeV/c (table 3 of [39]), a total flux of ∼2.6 particles per cm^2 min^{-1} is calculated for the sum of mu+ and mu− components. (Tsukaba, 30 m, BESS-02); Motoki *et al* [40], reported the total muon flux of ∼2.5 particles per cm^2 min^{-1} for Tsukuba, Japan (30 m), in BESS 1995 and a total muon flux of ∼2.6 particles per cm^2 min^{-1} for Lyne Lake, Canada (360 m), BESS 1997–1999, 1000 g cm^{-2}; Keramer *et al* [41] reported the total muon flux of ∼3.3 particles per cm^2 min^{-1} for Lyne Lake, Manitoba, Canada (56.5°N, 101.0°W, 360 m), in CAPRICE94, 1000 g cm^{-2}

and a total muon flux of ∼4.4 particles per cm^2 min^{-1} were reported by this group for Fort Summer, New Mexico (34.3°N, 104.1°W, 1270 m), CAPRICE97, 886 g cm^{-2}.

Other experiments were also providing data for different zenith angles essentially at sea level. For example record of near vertical muon in momentum range of 5–1200 GeV/c was done by Nandi and Sinha [42]. They reported a muon flux of ∼1.2 particles per cm^2 min^{-1} for Durgapur, India (110 m, 0°–0.3° zenith angle). Flux of near vertical muon in momentum range of 20–500 GeV/c, by Ayre *et al* [43]. A muon flux of ∼0.43 particles per cm^2 min^{-1} for Durham, MARS (0°–0.08° zenith angle) was reported by this group. In momentum range of 50–1700 GeV/c, Kellogg *et al* [44] reported flux of ∼0.23 and ∼0.53 particles per cm^2 min^{-1} for zeniths of 30° and 75°, respectively (Brookhaven National Laboratory). And in energy range of 1–1000 GeV, Jokisch *et al* [45] reported a flux of ∼1.1 particles per cm^2 min^{-1} for zeniths of 68°−82° (KIEL-DESY collaboration, Hamburg). In comparison, the reported fluxes by [42–44] and [45] are lower because they essentially report fixed zenith angle experiments or the flux within few degrees (i.e. 68°–82° from Jokisch *et al* [45], compared with [39–41]).

The reported value by our astronomical CCD was 0.83 and due to simulation it is about the half of the muons at this altitude. Thus the value is ∼1.6 particles per minute per square centimeter. The aluminum plates are not affected the result so much as the value of energy lose in aluminum just can reduce low energy muons (with energies lower than 1 GeV), this is about 8% of the total muon component.

Acknowledgments

This work has been supported financially by Iranian Space Agency (ISA) under the research project No. EX-RES11X and by Research Institute for Astronomy and Astrophysics of Maragha (RIAAM) under the research project No. 1/4165-24.

ORCID iDs

Pantea Davoudifar https://orcid.org/0000-0001-8359-6185
Zahra Bagheri https://orcid.org/0000-0002-3877-0882

References

[1] Gaisser T K 1990 *Cosmic Rays and Particle Physics* (Cambridge: Cambridge University Press)
[2] Wheeler J A 1949 Some consequences of the electromagnetic interaction between μ^--mesons and nuclei *Rev. Mod. Phys.* **21** 133
[3] De Pascale M P *et al* 1993 Absolute spectrum and charge ratio of cosmic ray muons in the energy region from 0.2 GeV to 100 GeV at 600 m above sea level *J. Geophys. Res.* **98** 3501
[4] Groom D 2002 Cosmic rays and other nonsense in astronomical CCD imagers *Exp. Astron.* **14** 45–55
[5] Acero M A *et al* 2019 Observation of seasonal variation of atmospheric multiple-muon events in NOvA near detector *Phys. Rev.* D **99** 122004
[6] Arunbabu K P *et al* 2017 Dependence of muon intensity on the atmospheric temperature measured by the GRAPES-3 experiment *Astropart. Phys.* **94** 22–8
[7] Kuno Y and Okada Y 2001 Muon decay and physics beyond the standard model *Rev. Mod. Phys.* **73** 151–202
[8] Kajita T 2012 Atmospheric neutrinos *Adv. High Energy Phys.* **2012** 504715
[9] Bailey R *et al* 1983 First measurements of efficiency and precision of CCD detectors for high energy physics *Nucl. Instrum. Methods Phys. Res.* **213** 201–15

[10] Iodache D A, Sterian P E and Tunaru I 2013 Charge coupled devices as particle detectors *Adv. High Energy Phys.* **2013** 425746
[11] Saoud T S, Moindjie S, Munteanu D and Autran J-L 2016 *Natural Radiation Events in CCD Imagers at Ground Level, Microelectronics Reliability* vol 64 (Amsterdam: Elsevier) pp 68–72
[12] Engvold O and Harvey J W (ed) 2001 *Physics of the Solar Corona and Transition Region* (Berlin: Springer) p 230
[13] Janesick J R 2011 *Scientific Charge Coupled Devices* vol 51 (Bellington, WA: SPIE Press) pp 670–5
[14] Falk E *et al* 1991 CCD camera readout system developments for HEP experiments at CERN *IEEE Nuclear Science Symp. and Medical Imaging Conf. (Santa Fe, NM, USA, 2–9 November 1991)* (https://doi.org/10.1109/nssmic.1991.258881)
[15] Heck D and Pierog T 2010 Extensive Air Shower Simulation with CORSIKA: A User's Guide (Version 6.960 from 23 March 2010)', Institute fur kernphysik, KARLSRUHER INSTITUT FUR TECHNOLOGIE (KIT)
[16] Integrated Surface Database Station History 2015 ftp://ftp.ncdc.noaa.gov/pub/data/noaa/
[17] https://data.irimo.ir/withoutlogin/index.aspx
[18] Heck D, Knapp J, Capdevielle J N, Schatz G and Thouw T 1998 *CORSIKA: A Monte Carlo Code to Simulate Extensive Air Showers* (Karlsruhe: Forschungszentrum Karlsruhe GmbH) p 6
[19] ICX259AL Datasheet by SONY
[20] The QHY6 CCD camera and CCDCap v2.6.2 http://nicolas.dupontbloch.free.fr
[21] Groom D E, Holland S E and Palio N P High resolution silicon detectors for 1.2–3 eV (400–1000) photon *Calorimetry in Particle Physics: Proc. 11th Int. Conf.* pp 21–4
[22] FV: The Interactive FITS File Editor https://heasarc.gsfc.nasa.gov/docs/software/ftools/fv/
[23] https://exelisvis.com/
[24] Lauss B *et al* 1996 Excited state muon transfer in hydrogen/deuterium mixtures *Phys. Rev. Lett.* **76** 4693–6
[25] Groom D 2004 Cosmic rays and other nonsense in astronomical CCD images *Scientific Detectors for Astronomy: The Beginnings of a New Era* (Dordrecht: Kluwer) p 83
[26] Hopkinson G R 1994 Radiation effects on solid state imaging devices *Radiat. Phys. Chem.* **43** 79–91
[27] Heijne E H M 1986 The use of semiconductor imagers in high energy particle physics *Proc. SPIE* **0591**
[28] Smith A R *et al* 2002 Radiation events in astronomical CCD images, sensors and camera systems for scientific, industrial, and digital photography applications III *Proc. SPIE* **4669** 172–83
[29] Kalmykov N N and Ostapchenko S S 1993 *Yad.Fiz.* **56** 105
[30] Fesefeldt H 1985 *The Simulation of Hadronic Showers-Physics and Applications* RWTH Aachen Report No PITHA85/02 RWTH Aachen University
[31] Alcaraz J *et al* 2000 Protons in near Earth orbit *Phys. Lett.* B **472** 215–26
[32] Gaisser T K 2006 The cosmic-ray spectrum: from knee to ankle *J. Phys.: Conf. Ser.* **47** 15–20 and references therein
[33] Bobik P *et al* 2012 Distribution of secondary particles intensities over Earth's surface: effect of the geomagnetic field *Adv. Space Res.* **50** 986–96
[34] Lin J W *et al* 2010 *Nucl. Instrum. Methods Phys. Res.* A **619** 24–7
[35] Dimitrieva A N *et al* 2005 *29th Int. Cosmic Ray Conf.* vol 6 *(Pune)* pp 73–6
[36] Grieder P K F 2001 *Cosmic Rays at Earth* (Amsterdam: Elsevier Science)
[37] Mackay C D 1986 *Ann. Rev. Astron. Astrophys.* **24** 255–83 See especially p 268
[38] Florentin-Nielsen R, Andersen M I and Nielsen S P 1995 Cosmic ray events and natural radioactivity in CCD cryostats *New Dev. Array Technol. Appl.; IAU Symp.* 167 *(The Hague, the Netherlands, 23–27 Aug)*
[39] Haino S *et al* 2004 Measurements of primary and atmospheric cosmic-ray spectra with the BESS-TeV spectrometer *Phys. Lett.* B **594** 35–46
[40] Motoki M *et al* 2003 Precise measurements of atmospheric muon fluxes with the BESS spectrometer *Astropart. Phys.* **19** 113–26
[41] Kremer J *et al* 1999 Measurements of ground-level muons at two geomagnetic locations *Phys. Rev. Lett.* **83** 4241–4
[42] Nandi B C and Sinha M S 1972 The momentum spectrum of muons at sea level in the range 5–1200 Gev/c *J. Phys. A: Gen. Phys.* **5** 1384–94

[43] Ayre C A *et al* 1975 Precise measurement of the vertical muon spectrum in the range 20–500 Gev/c *J. Phys. G: Nucl. Phys.* **1** 584–600
[44] Kellogg R G and Kasha H 1978 Momentum spectra, charge ratio, and zenith-angle dependence of cosmic ray muons *Phys. Rev.* D **17** 98–113
[45] Jokish H, Carstensen K, Dau W D, Meyer H J and Allkofer O C 1979 Cosmic ray muon spectrum up to 1 TeV at 75° zenith angle *Phys. Rev.* D **19** 1368–72